Finite Larmor Radius Effects on Transport Barriers in Plasmas with Zonal Flows

J. J. Martinell[1], D. del-Castillo-Negrete[2]

[1]*Instituto de Ciencias Nucleares, UNAM, A. Postal 70-543, México D.F., Mexico*

[2]*Oak Ridge National Laboratory, Oak Ridge, TN 37831-6169, USA*

I. Introduction. The appearance of transport barriers in plasmas in relation to sheared flows has been studied since the discovery of the H-mode three decades ago, based on the premise that an increased shear leads to turbulence suppression. This gives rise to barriers for turbulent transport but is also known that barriers to chaotic transport can arise in regions of zero shear [1]. The presence of these barriers is linked to non-twist Hamiltonian systems which provide a description of transport for particles under the EXB drift approximation. The studies so far have been based on the guiding center description which assumes zero Larmor radius. However, the effect of finite Larmor radius (FLR) should be of importance for the high temperature ITER-like plasmas and especially for fusion-generated alpha particles.

Here we study chaotic transport in non-monotonic zonal flows taking into account FLR effects. The results found for zero Larmor radius can be summarized as follows: (a) shearless regions of the zonal flow contain transport barriers, (b) fluctuations related to drift waves destroy invariant surfaces that contain particles, (c) the shearless surface is very robust and is the last to break, for high fluctuation levels.

II. Gyroaverage particle model.

The model is based on a test particle subject to the EXB drift velocity, which assumes the particle follows the guiding center velocity. For finite gyroradii the particle actually samples spatial regions around the guiding center and this effect can be accounted by taking the average of the drift equations over the gyroradius. Thus, the equations are

$$\frac{dx}{dt} = -\left\langle \frac{\partial \phi}{\partial y} \right\rangle_\theta , \qquad \frac{dy}{dt} = \left\langle \frac{\partial \phi}{\partial x} \right\rangle_\theta \tag{1}$$

where the gyroaverage, $\langle\,\rangle_\theta$, is defined as $\langle \Psi \rangle_\theta \equiv \frac{1}{2\pi}\int_0^{2\pi} \Psi(x+\rho\cos\theta, y+\rho\sin\theta)\,d\theta$. This represents a Hamiltonian system with $\langle\phi\rangle_\theta$ as the Hamiltonian. In our model $\phi = \phi_0 + \phi_1$ where ϕ_0 is the zonal flow, given by $\hat{u}_0(x) = \frac{d\phi_0}{dx} = \mathrm{sech}^2 x$, and the fluctuations ϕ_1 are given by two modes of the Hasegawa-Mima equation, in the co-moving frame of one mode. Its gyroaverage is,

$$\langle\phi\rangle_\theta = J_{0\rho}(x) - \eta x + \varepsilon_1 J'_{k_1\rho}(x)\cos(k_1 y) + \varepsilon_2 J'_{k_2\rho}(x)\cos(k_2 y - \omega t)\,, \tag{2}$$

where the prime denotes the derivative of the function $J_{k\rho}(x)$, which is defined by,

$$J_{k,\rho}(x) = \frac{1}{\pi}\int_0^{\pi} \tanh\left(x+\rho\cos\theta\right)\cos\left(k\rho\sin\theta\right)d\theta\,. \tag{3}$$

For small ρ it is,

$$J_{k,\rho}(x) = \left[1-\frac{\rho^2}{2}\left(\mathrm{sech^2 x}+\frac{\mathrm{k}^2}{2}\right)\right]\tanh x+\mathscr{O}(\rho^3)\,. \tag{4}$$

The equations 1 with 2 are integrated to determine the particle evolution. The phase space (in our case the $x-y$ space) topology of this system can be analyzed for $\varepsilon_2 = 0$. In general, it is characterized by two resonances on each side of the shearless point, where the mode velocity equals the flow velocity. For $\rho = 0$ the resonances can form two separate chains of islands (heteroclinic, when wave amplitude is low) or they can join in coupled chains (homoclinic, for large wave amplitude). For finite ρ two interesting results are found [2]: as ρ increases (a) there is a bifurcation of the shearless curve corresponding to the effective flow profile transiting from a single maximum to two maxima and a minimum, and (b) the topology changes from heteroclinic to homoclinic by means of separatrix reconnection.

III. Chaotic transport. When the time dependent term is included ($\varepsilon_2 \neq 0$) the system in non-integrable and invariant surfaces can break up leading to chaotic trajectories. The results can be presented as Poincaré surface of section plots in order to follow the particles in the $x-y$ plane and monitor their radial displacements (x direction here). The particle crosses the surface of section every wave period ($T = 2\pi/\omega$). When $\rho = 0$ as the amplitude ε_2 increases more and more trajectories become chaotic until the shearless surface itself turns chaotic and global chaos is set, which means the transport barrier has disappeared. The FLR effect on transport can be seen in Fig.1 for hetroclinic case. For large enough $\varepsilon_2 = 0.05$ the transport is chaotic for zero Larmor radius but as ρ increases the trajectories become more regular until the transport barrier is restored. Since, the shearless curve (SC) is the most robust we can determine the point of barrier break-up by tracking the behavior of this curve. This can be made using the indicator points (IP) method [3]. The IP are defined in terms of the evolution operator given by the solution of Eqs. (1) at time t and the symmetry transformations obeyed by the system $S:\{x' = -x; y' = y+\pi/k_1\}$ and $I_0:\{x' = x; y' = -y\}$, noting that, for the period T, $G_T = I_1 I_0$, where the involution $I_1 = G_T I_0$. Then the IP satisfy $I_0(x,y) = S(x,y)$ or $I_1(x,y) = S(x,y)$, or equivalently $G_T(x,y) = SI_0(x,y) = (-x,-y+\pi/k_1)$. The IP are part of the SC so they can be iterated with the operator G_T in order to create a Poincaré section of the SC. We follow the method in [4] to find the IP and the resulting SC is shown in Fig.2 for heteroclinic topology,

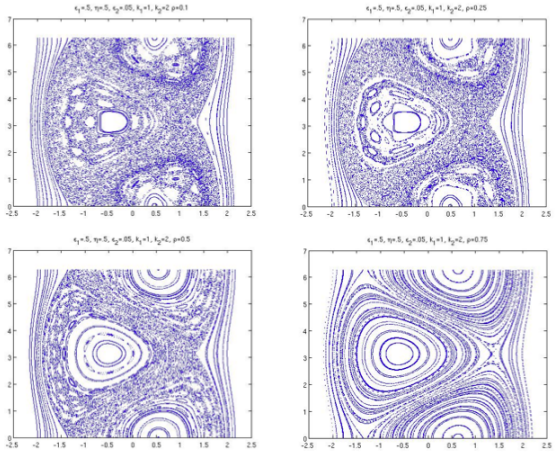

Figure 1: Gyro-phase average induced chaotic transport suppression for heteroclinic topology.

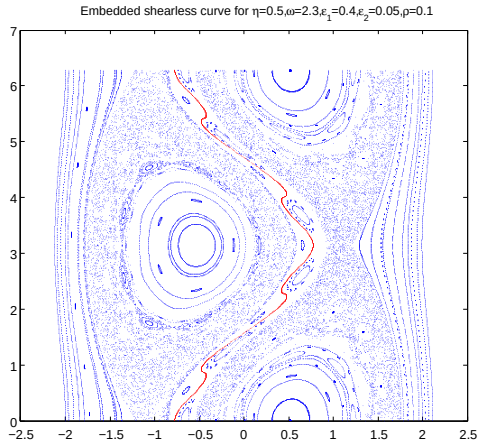

Figure 2: Shearless curve (red) together with chaotic particle trajectories, showing it forms a region where the particles cannot cross.

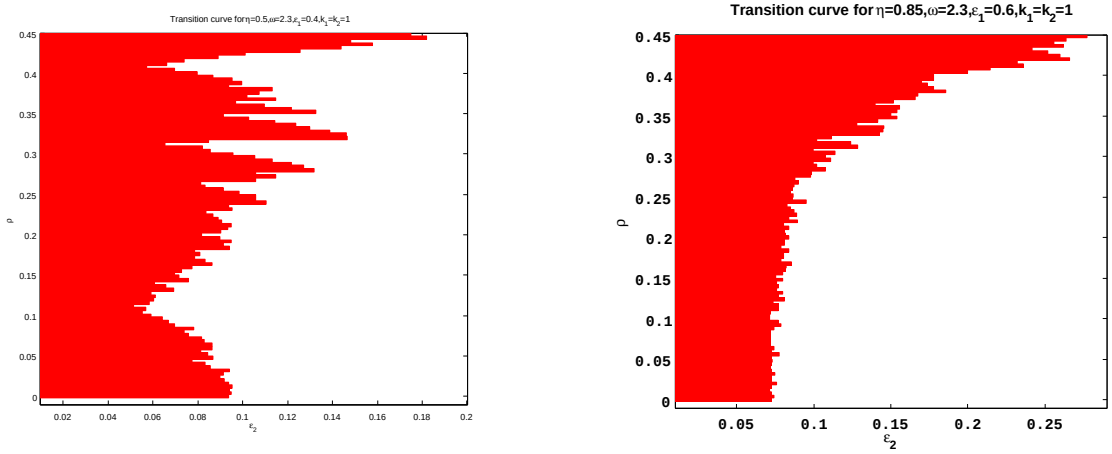

Figure 3: Threshold for the destruction of the shearless curve for (a) heteroclinic geometry when $\rho = 0$ and (b) homoclinic geometry at $\rho = 0$.

embeded in the chaotic map, but still unbroken. Similar results are found for the homoclinic case.

The SC becomes chaotic for certain value of ε_2 at which point transport barriers disappear. The effect of FLR on the break-up of the SC can be seen in Fig.3 where we have determined the values of ρ and ε_2 for which the SC ceases to exist, for both topologies (at $\rho = 0$). This diagram is similar to the bird-wing of Refs.[3,4], and exhibits an irregular threshold of a fractal type.

Next we examined the transport barrier effectiveness over a thermal distribution of particles. For this we take a Maxwellian distribution of Larmor radii and follow them from an initial region about the separatrix X-point. The fraction of particles crossing the SC is shown in Fig.4 for parameters corresponding to what would be hetroclinic and homoclinic topologies at $\rho = 0$.

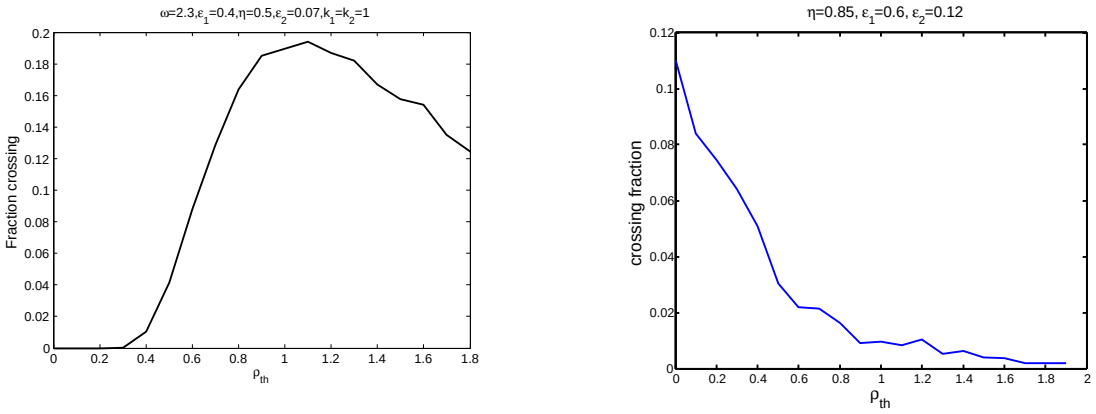

Figure 4: Fraction of thermal particles crossing from one side to the other of the barrier that would be present when $\rho = 0$, corresponding to (a) heteroclinic geometry when $\rho = 0$ and (b) homoclinic geometry at $\rho = 0$.

Finally, the nature of transport in the poloidal (y) direction can be analyzed by following a group of particles about the X-point. Some particles follow the zonal flow, others are trapped within an eddy and a third group (sticky-flight) alternates between eddies and zonal flow. We isolate the later and compute the mean M and variance σ^2 of the y-displacement. The time scaling, $M \sim t^{\chi}$, $\sigma^2 \sim t^{\gamma}$, determines the nature of transport. Fig.5 shows that $\chi \approx 1$, meaning normal convection, but $\gamma > 1$ indicating superdiffusive transport. Using the approximation eq.4, we find that $\gamma = 1.7$ for heteroclinic and $\gamma = 1.73$ for homoclinic cases but they are the same for all values of ρ. So, FLR effects seem to be unimportant for y-transport to this approximation.

Acknowledgements. This work was partially supported by DGAPA-UNAM IN106911 and CONACyT 152905 Projects.

References

[1] D. del-Castillo-Negrete, Phys. Plasmas **7**, 1702 (2000).

[2] D. del-Castillo-Negrete and J.J. Martinell, Comm. Nonlinear Sci. Numerical Simul. 17, 2031 (2012).

[3] S. Shinohara and Y. Aizawa, Prog. Theor. Phys. **97**, 379 (1997).

[4] M. V. Budyansky, M. Yu. Uleysky, and S. V. Prants, Phys. Rev. E, **79**, 056215 (2009).

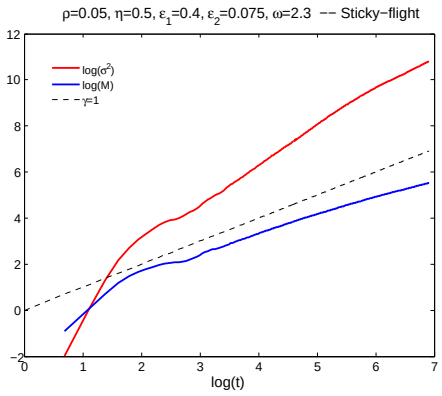

Figure 5: Scaling of σ^2 and the mean M.